SHORT REPORT

WILEY

A revised order of subunits in mammalian septin complexes

Deborah C. Mendonça[1†] | Joci N. Macedo[1,2†] | Samuel L. Guimarães[1] |
Fernando L. Barroso da Silva[3,4] | Alexandre Cassago[5] | Richard C. Garratt[1] |
Rodrigo V. Portugal[5] | Ana P. U. Araujo[1]

[1]São Carlos Institute of Physics, USP, São Carlos, SP, Brazil

[2]Federal Institute of Education, Science and Technology of Rondonia

[3]Faculty of Pharmaceutical Sciences, USP, Ribeirão Preto, SP, Brazil

[4]UMR_S 1134, Université Paris Diderot, Paris, France

[5]Brazilian Nanotechnology National Laboratory, CNPEM, Campinas, SP, Brazil

Correspondence
Rodrigo V. Portugal, Brazilian Nanotechnology National Laboratory, CNPEM, Campinas, SP, Brazil.
Email: rodrigo.portugal@lnnano.cnpem.br

Ana P. U. Araujo, São Carlos Institute of Physics, USP, São Carlos, SP, Brazil.
Email: anapaula@ifsc.usp.br

Funding information
Fundação de Amparo à Pesquisa do Estado de São Paulo, Grant/Award Numbers: 2014/15546-1, 2015/16116-3, 2017/15340-2

Abstract

Septins are GTP binding proteins considered to be novel components of the cytoskeleton. They polymerize into filaments based on hexameric or octameric core particles in which two copies of either three or four different septins, respectively, assemble into a specific sequence. Viable combinations of the 13 human septins are believed to obey substitution rules in which the different septins involved must come from distinct subgroups. The hexameric assembly, for example, has been reported to be SEPT7–SEPT6–SEPT2–SEPT2–SEPT6–SEPT7. Here, we have replaced SEPT2 by SEPT5 according to the substitution rules and used transmission electron microscopy to demonstrate that the resulting recombinant complex assembles into hexameric particles which are inverted with respect that predicted previously. MBP-SEPT5 constructs and immunostaining show that SEPT5 occupies the terminal positions of the hexamer. We further show that this is also true for the assembly including SEPT2, in direct contradiction with that reported previously. Consequently, both complexes expose an NC interface, as reported for yeast, which we show to be more susceptible to high salt concentrations. The correct assembly for the canonical combination of septins 2-6-7 is therefore established to be SEPT2–SEPT6–SEPT7–SEPT7–SEPT6–SEPT2, implying the need for revision of the mechanisms involved in filament assembly.

KEYWORDS
core particle complex, NC interface, septin, TEM

1 | INTRODUCTION

Septins belong to the family of P-loop GTPases (Weirich, Erzberger, & Barral, 2008). They differ from most other members in their ability to polymerize into filaments, a property which is the result of a characteristic sequence known as the Septin Unique Element (Valadares, Pereira, Araujo, & Garratt, 2017; Versele et al., 2004). Septins have been classically described to participate in cytokinesis, but also play roles in other important intracellular processes. These include acting

as scaffolds in the recruitment of binding partners; as diffusion barriers in the compartmentalization of membrane proteins; in host–microorganism interaction and even in mechanotransduction (Caudron & Barral, 2009; Gladfelter, Pringle, & Lew, 2001; Lam & Calvo, 2018; Mostowy & Cossart, 2012).

Structurally, septins are divided into three principal domains: the N-terminal (N), GTP-binding (G), and C-terminal (C) domains. The central, G domain, is the most conserved and its ability to bind GTP is important for the interaction between septins within filaments and is fundamental to ensure structural integrity (Valadares et al., 2017; Zent & Wittinghofer, 2014; Zeraik et al., 2014). Based on sequence

---

[†]Deborah C. Mendonça and Joci N. Macedo contributed equally to this work.

similarity, the 13 mammalian septins have been subdivided into four distinct groups (Kinoshita, 2003; Nishihama, Onishi, & Pringle, 2011; Pan, Malmberg, & Momany, 2007). Representatives of either three or all four of the groups combine to form linear oligomeric core complexes, which assemble end-to-end into filaments and thence into higher-order structures (Beise & Trimble, 2011; Sirajuddin et al., 2007). Similar observations have been made for other species where the exact number of different septins involved may vary (Bertin et al., 2008; Field et al., 1996; Frazier et al., 1998; John et al., 2007).

It is well established that septin filaments can be broken down into their corresponding core complexes under conditions of high ionic strength (Field et al., 1996; Frazier et al., 1998; Kinoshita, 2003). To date, the best description of such a complex is that of the linear hexameric particle formed of two copies each of human septins 2, 6, and 7 (Sirajuddin et al., 2007). Each septin monomer participates in two interfaces which alternate along the filament: the NC interface, involving the N and C terminal helices of the G domains; and the G interface, including the region directly involved in guanine-nucleotide-binding (Sirajuddin et al., 2007; Valadares et al., 2017). The remaining domains (particularly the coiled coil region of the C-domain) also contribute to the affinity and specificity of the NC interface (Barth, Schoeffler, & Alber, 2008; de Marques et al., 2012; Sala, Valadares, Macedo, Borges, & Garratt, 2016; Versele et al., 2004).

Sirajuddin et al. (2007), using negative-stain electron microscopy and employing a version of SEPT2 fused to MBP, proposed that SEPT2 occupies the central position of the core complex and SEPT7 lies at its extremities, leading to the following arrangement for the hexamer: SEPT7–SEPT6–SEPT2–SEPT2–SEPT6–SEPT7 (which, for convenience, we will abbreviate to 7-6-2-2-6-7). This arrangement leaves a G-interface free at each end of the particle and has widely been considered to be a true description of the hexamer since the publication of the original crystal structure (Sirajuddin et al., 2007). Subsequent studies have shown the existence of octameric core particles which incorporate SEPT9 (Kim, Froese, Estey, & Trimble, 2011; Sandrock et al., 2011; Sellin, Sandblad, Stenmark, Gullberg, & Kellogg, 2011). In this case, it has been assumed that SEPT9 occupies the terminal position by forming a G interface with SEPT7. As a consequence, the octameric core particle exposes NC interfaces at its termini as is the case for yeast (Bertin et al., 2008).

Kinoshita (2003) proposed that any given septin could be substituted by another from the same group, generating a physiologically viable combination. This hypothesis allows for the prediction of the position of any particular septin within the core complex and limits the number of possible combinations to 20 for hexamers and 60 for octamers. However, the generality of Kinoshita's hypothesis is not yet fully established. On the one hand, most of the theoretically possible combinations have yet to be described in vivo and on the other, there have been reports of complexes which are incompatible with its basic premise (Lukoyanova, Baldwin, & Trinick, 2008; Nagata, Asano, Nozawa, & Inagaki, 2004). In summary, the rules governing core complex and filament assembly are far from fully established.

In order to enhance our current knowledge concerning septin heterocomplexes, we have selected a combination composed of SEPT5, SEPT6, and SEPT7 for more detailed molecular characterization. This choice was made based on two criteria. First, previous experiments have shown the existence of such a complex in platelets where it associates with microtubules and plays an important role in granule trafficking (Martínez et al., 2006; Neubauer & Zieger, 2017). Second, it is a conservative choice as it represents a minimal alteration when compared to the canonical SEPT2–SEPT6–SEPT7 complex. The substitution of SEPT2 by SEPT5, which belong to the same subgroup, is in accordance with Kinoshita's predictions. Unexpectedly, we show that both of the hexameric core complexes are inverted with respect to that reported previously suggesting the need for a critical revision of the septin literature.

2 | RESULTS AND DISCUSSION

2.1 | Characterization of the SEPT5–SEPT6–SEPT7 heterocomplex

In order to investigate the prediction of Kinoshita (2003) that SEPT5 should be able to replace SEPT2 as a component of a viable heterocomplex, we co-expressed SEPT5, SEPT6 and SEPT7 in *Escherichia coli* Rosetta (DE3) cells. SEPT5 was produced with or without an MBP-tag and an N-terminal His-tag was added to SEPT7 to facilitate purification by metal affinity chromatography. Size exclusion chromatography proved essential for eliminating aggregates and contaminants, yielding a symmetrical peak corresponding to the stoichiometric SEPT5–SEPT6–SEPT7 complex (Figure 1a). The identity of all components was confirmed by mass spectrometry.

2.2 | SEPT5–SEPT6–SEPT7 complex is a hexamer

Transmission electron microscopy revealed that the complex formed by SEPT5, SEPT6, and SEPT7 is a linear hexamer in which the six individual monomers can be clearly resolved (Figure 1c,d). This result was anticipated since SEPT5 belongs to the same subgroup as SEPT2, which also forms hexamers together with SEPT6 and SEPT7. In addition, the 25 nm length of the particle agrees well with that of the SEPT2–SEPT6–SEPT7 hexamer, inferred from its crystal structure (Sirajuddin et al., 2007). The ratio of GDP to GTP bound to this complex was 2:1 (Figure 1b), which is consistent with that found for the SEPT2–SEPT6–SEPT7 complex (Sirajuddin et al., 2007) and with the lack of catalytic activity associated with SEPT6.

2.3 | SEPT5 shows an unexpected position in the hexamer

According to Kinoshita's predictions, SEPT5 is expected to be found at the position normally occupied by SEPT2 in the canonical complex (2-6-7) since they belong to the same subgroup (Kinoshita, 2003). To test this hypothesis, TEM images of negatively stained complexes containing MBP-SEPT5 were collected and processed. Due to the flexible linker, the relative position of the MBP with respect to the hexamer was expected to be variable and it was therefore essential to
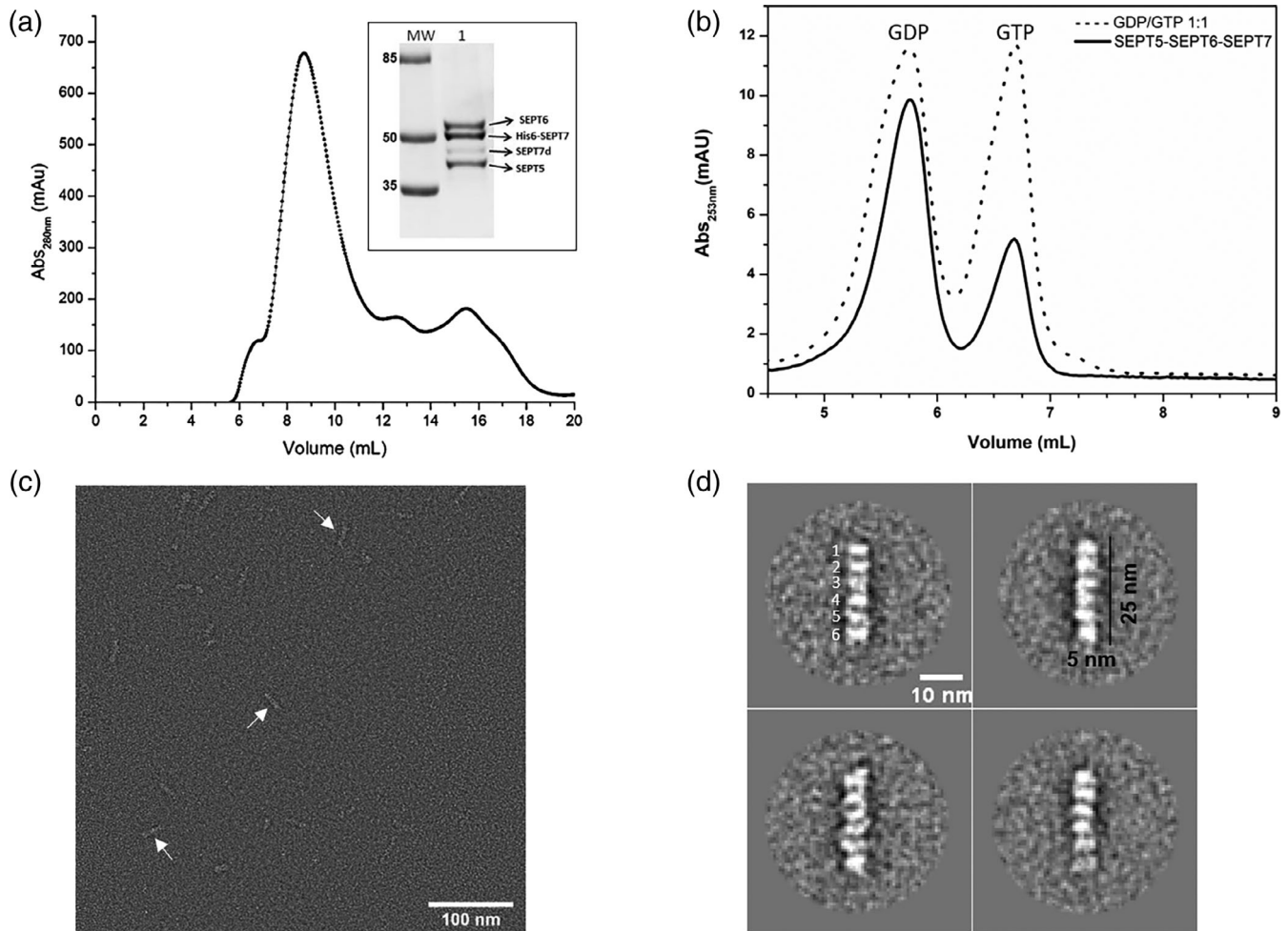
FIGURE 1 Characterization of the human SEPT5–SEPT6–SEPT7 complex. (a) Size exclusion chromatography in which the major peak corresponds to the hexameric complex. The inset shows a 12%SDS-PAGE including a molecular mass standard, MW (in kDa) and (1) the major peak from the size exclusion column. All three septins can be identified. An extra, weak band (SEPT7d) corresponding to 6xHis-SEPT7 lacking part of the C-domain due to degradation was regularly observed during purification, similar to that described by Sirajuddin et al. for the SEPT2–SEPT6–SEPT7 complex (Sirajuddin, 2007). (b) Elution profile of guanine nucleotides from 2.4 μM of denatured purified complex. The sample was analyzed by HPLC on a DEAE-5PW anion-exchange column and monitored at 253 nm. A mixture containing 5 μM of both GTP and GDP was used as a reference (dotted line); AU, absorbance units. (c) Electron micrograph of the purified complex at high salt concentration (800 mM). Arrows indicate hexameric particles. (d) Four representative class averages (~30 particles each) derived from processing a total of 18,000 particles from the micrographs

use a rectangular mask that would eliminate the dominant effect of the septin complex during the classification process. Classes were therefore identified as a function of the position of the MBP, which is not expected to be observed simultaneously at both ends of the particle in most class average due to the fact that there is no correlation between their positions. A second mask was therefore employed in order to classify particles based on the position of the MBP at only one end of the complex. Different strategies were used during processing and in all cases the results showed MBP situated in variable positions centered on the end of the hexameric complex (Figure 2a). This implies that SEPT5 occupies the terminal position within the complex, in direct contrast to that expected based on the currently accepted model for the canonical hexamer, 7-6-2-2-6-7 (and by implication 7-6-5-5-6-7). For the reasons given above the class

averages shown in Figure 2a show MBP associated with only one end of the complex. Nevertheless, if the second mask is omitted during data processing then, on rare occasions, it is possible to observe classes of particles in which both MBPs are simultaneously visible (Figure 2c).

Although convincing, the unexpected nature of this result together with concerns about the flexibility of the linker between the MBP and SEPT5 led us to propose a new experiment to confirm its position. For this, a specific antibody was used to label SEPT5 (lacking MBP) within the complex. Examination of the raw images of particles from these micrographs confirmed the location of SEPT5 at the end of the hexamer, as shown in Figure 2b. In some cases, a single antibody is observed interacting with one end of the hexamer and in others an antibody crosslinks two hexamers.
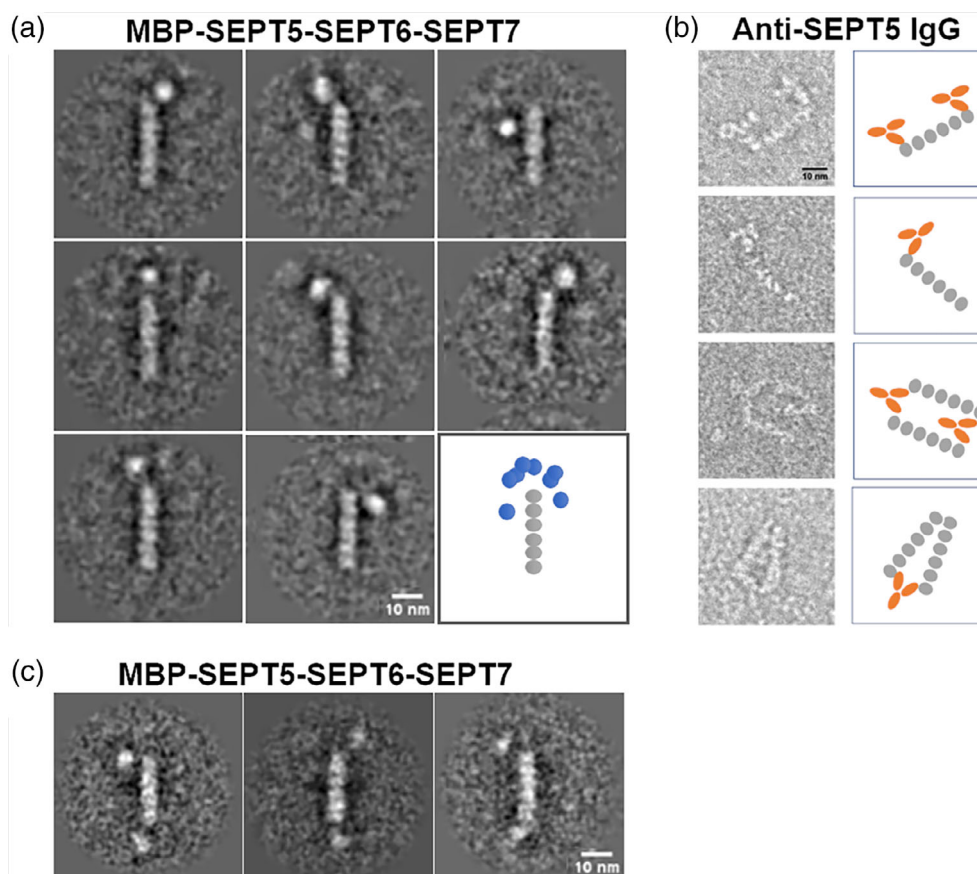
FIGURE 2 Location of MBP-SEPT5 and antibody decoration. (a) Representative class averages (~30 particles each) of purified MBP-SEPT5–SEPT6–SEPT7 at high salt concentration (800 mM). The extra density is most often positioned close to the end of the rods. On the bottom right is shown a schematic of the superimposed class averages showing the terminal monomer of the hexamer to lie at the center of the arc defined by the different MBP positions. (b) Left, four representative raw (unaveraged) images of the sample prepared with purified human SEPT5–SEPT6–SEPT7 complex incubated with mouse anti-SEPT5 antibody at 500 mM NaCl. Right, schematic diagram of the complexes, where gray represents septin subunits and orange the antibody. (c) Three examples of class averages showing MBP bound to both ends of the hexamer [Color figure can be viewed at wileyonlinelibrary.com] [Color figure can be viewed at wileyonlinelibrary.com]

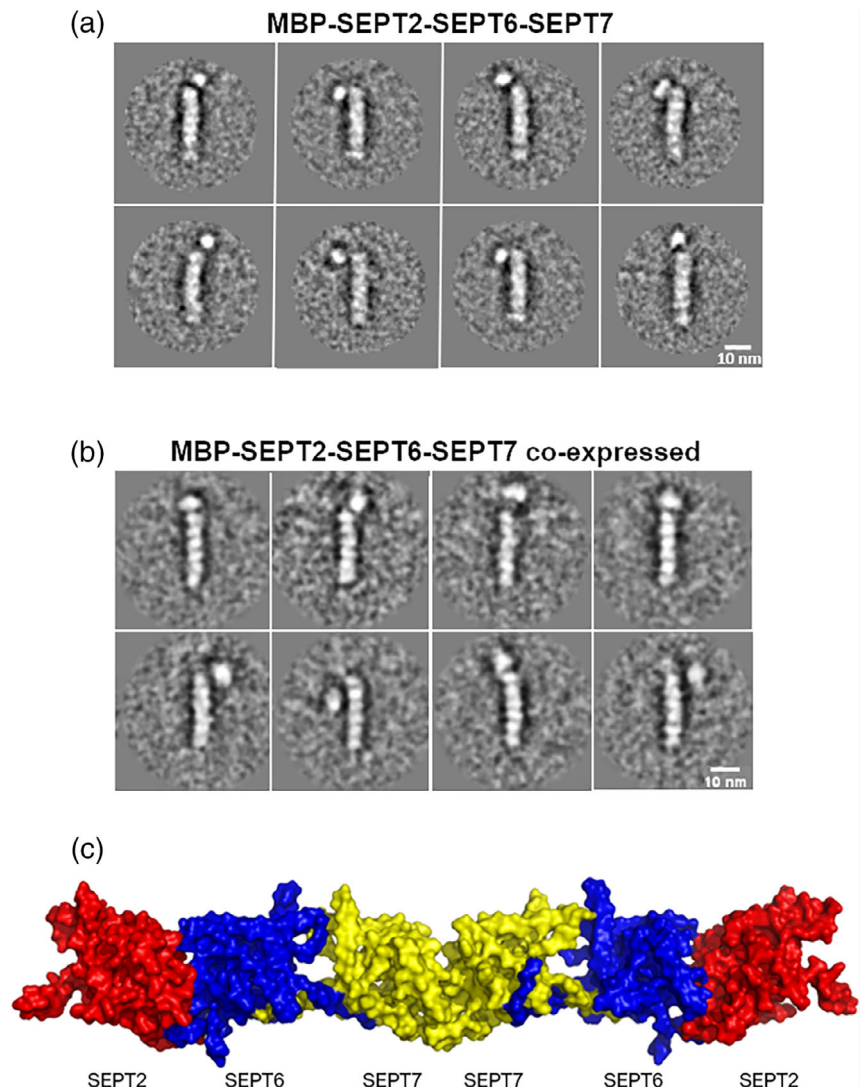## 2.4 | Reviewing the position of SEPT2 in the core complex

The unexpected arrangement of the 5-6-7 hexamer suggested two possibilities; either the substitution of SEPT2 by SEPT5 leads to a genuinely different assembly or the currently accepted model is wrong. To distinguish between these possibilities, analogous TEM studies were undertaken using the canonical 2-6-7 complex, once again employing a construct in which MBP was fused to SEPT2, as per Sirajuddin et al. (2007). In this case the full complex was assembled by mixing cells which independently expressed either SEPT7 or both MBP-SEPT2 and SEPT6 together. Figure 3a shows eight representative class averages in which the MBP is clearly visible close to the extremity of the core complex indicating that SEPT2 also occupies the terminal position. Given that this complex was produced in a slightly different way to that of 5-6-7 (in which MBP-SEPT2 and SEPT6 were coexpressed and then united with SEPT7) we considered it important to test if this could affect the final assembly of the hexamer. A sample in which MBP-SEPT2, SEPT6, and SEPT7 were all coexpressed in the same cells was therefore produced and the corresponding complexes

examined using TEM. The final class averages (Figure 3b) show the same result as previously and demonstrate that spontaneous assembly is robust and independent of the methodology employed.

The results from both complexes are therefore coherent with Kinoshita's proposition (namely that SEPT2 and SEPT5 occupy equivalent positions) but clearly indicate that the structural model originally proposed is incorrect. It is therefore of interest to ask how such a mistake may have arisen.

In the crystal structure of the human 2-6-7 complex the asymmetric unit consists of a trimer organized in the following manner; SEPT2–SEPT6–SEPT7, in which a G interface is formed between SEPT2 and SEPT6 and an NC interface between SEPT6 and SEPT7 (Sirajuddin et al., 2007). From this trimer, the hexameric core complex (as observed with TEM under high salt conditions) could be generated by either of two crystallographic twofold axes leading to the following alternative arrangements, 7-6-2-2-6-7 or 2-6-7-7-6-2. The authors used an MBP-SEPT2 construct together with single particle analysis in order to define the boundaries of the particle, leading to the conclusion that SEPT2 was located at the center of the hexamer leaving

FIGURE 3 Location of SEPT2 determined by negative stain TEM using MBP-SEPT2. (a) Representative class averages (~30 particles each) of purified MBP2-6-7 human septin complex at high salt concentration (800 mM). The extra density (MBP) is positioned close to the end of the rods, as observed for MBP5-6-7. (b) A similar result is observed if the three septins are simultaneously coexpressed. (c) Revised structural model for the hexamer generated from PDB file 2QAG after appropriate application of crystallographic symmetry [Color figure can be viewed at wileyonlinelibrary.com] [Color figure can be viewed at wileyonlinelibrary.com]

(a) MBP-SEPT2-SEPT6-SEPT7

10 nm

(b) MBP-SEPT2-SEPT6-SEPT7 co-expressed

10 nm

(c)

SEPT2   SEPT6   SEPT7   SEPT7   SEPT6   SEPT2

SEPT7 exposed at its extremities. One difference between our studies and those reported previously is that Sirajuddin et al. used glutaraldehyde to fix the samples and made measurements at lower salt concentration. Furthermore, technological advances over the last decade have greatly enhanced the ease with which single particle images can be interpreted and on repeating this experiment we observe that, in fact, the hexamer is inside out with respect to that reported previously and the correct order of the subunits is therefore 2-6-7-7-6-2 (Figure 3c). Furthermore, two different approaches show that this is also the case for the core particle 5-6-7-7-6-5 in accordance with Kinoshita's proposal that septins from the same subgroup should be interchangeable (Kinoshita, 2003).

One important consequence of our observation is that the interface, which now lies exposed at the extremity of the core complex, is an NC interface rather than G. This is the interface which is susceptible to high salt concentrations leading to depolymerization under these conditions. This interface is therefore fundamental to the polymerization process and it has been shown in yeast that it is the formation of end-to-end contacts between core complexes via lateral

diffusion within the membrane which leads to polymerization (Bridges, Zhang, Mehta, Occhipinti, & Tani, 2014).

The question then arises as to which of the two interfaces would be expected to more labile—the SEPT7–SEPT7 G interface or the SEPT2–SEPT2 NC interface? PISA was used to analyze both. The G interface was taken directly from the high-resolution crystal structure of the SEPT7 G-domain (PDB ID 6N0B) and a model for the SEPT2 NC interface was generated from two incomplete crystal structures (PDB ID 2QNR and 2QA5). The two interfaces have approximately equal buried surface areas (1,677 and 1,651 $Å^2$ per subunit, respectively for NC and G) but the predicted binding energy of interaction is slightly more favorable for the G interface (−21.8 compared with −16.8 kcal/mol). The P-value, an indicator of the likelihood of a physiologically relevant interaction, is also more favorable for G than NC (0.29 compared with 0.55). Most notable, however, is that the number of charged residues involved in salt bridges at the interface is 9 at the NC interface but only 4 at the G interface. Many such interactions involve the polybasic region, which is tucked into the NC interface and stabilized by compensating charges from the neighboring subunit.

At high ionic strength, with an increased dielectric constant, this interface would be expected to be destabilized exposing the SEPT2 NC surface, consistent with the new model for the hexamer.

To test this further, Monte Carlo simulations were performed and used to determine the interaction energy of the two monomers at each interface as a function of their separation. Figure 4 shows how $-\beta\Delta G$ (a measure of interface stability) at the optimal separation decreases as a function of the NaCl concentration. The SEPT2–SEPT2 NC interface is markedly more sensitive to the salt concentration and is clearly less stable above about 100 mM. Once again, this indicates that depolymerization would be expected to occur preferentially by disruption of the SEPT2–SEPT2 NC interface rather than the SEPT7–SEPT7 G interface, consistent with exposing a SEPT2 NC interface at each end of the hexamer as we observe experimentally.

Furthermore, this proposal finds experimental support in the literature. For example, Zent and Wittinghofer (2014) describe the SEPT7 G-interface as being particularly stable and that this leads to very low hydrolytic rates as a consequence of slow GDP release. It is therefore very hard to imagine why a free SEPT7 G interface would remain exposed at the termini of the hexamer as in the original model. Perhaps more surprising is the fact that SEPT2 G-domains purify as homodimers which are stabilized by the G-interface rather than the physiological NC interface (Sirajuddin et al., 2007). Once again, these observations appear to highlight the fragility of the NC interface compared with G.

It is pertinent to note that the octameric core complex from yeast also presents an NC interface exposed at its termini and this is similarly salt sensitive (Figure 5c) (Bertin et al., 2008). In this octameric particle, there is an additional septin, Cdc10. This lacks the C-terminal coiled-coil domain and is located at the center of the complex. Therefore, in both the mammalian hexamer and the yeast octamer, rupture occurs at analogous positions, namely at the NC interface which

forms a homodimeric coiled coil (Figure 5c). Nevertheless, there are important differences between the two cases. For example, there is no strict equivalence in terms of catalytic activity. Human SEPT6 and cdc12 occupy the penultimate position of the octamer and yet the latter is active whilst the former is not. Clearly, further work is necessary in order to fully understand the relationship between catalytic activity and particle assembly.

Octameric complexes of human septins have also been reported. These include SEPT9, a member of the remaining subgroup which does not participate in the hexamer (Kim et al., 2011; Sellin et al., 2011). Cdc10 is evolutionarily closer to SEPT9 than to other mammalian septins and both lack the C-terminal coiled coil (Pan et al., 2007). However, it has been implied that SEPT9, which interacts strongly with SEPT7 would be located at the end of the core complex (Nakahira et al., 2010). This would be compatible with the standard model but not with that presented here and it is tempting to speculate that SEPT9, when present, would occupy the central position. If this were the case then the yeast and human octamers would display analogous architectures (Figure 5c). In vivo studies in yeast have shown that in the absence of Cdc10, a hexamer is rescued, which has Cdc11 (analogous to the SEPT2 subgroup) at the ends (McMurray et al., 2012). In this case, the central septin, Cdc3, forms a homotypic interaction via a G interface, forming a hexameric arrangement similar to the human complex proposed here (Figure 5d).

Our results change the current ideas concerning the assembly of septin filaments from their monomeric components and core complexes by placing SEPT7 at the center of the hexamer in both of the complexes studied (Figure 5b). These assemble in accordance with Kinoshita's proposal and it is therefore reasonable to assume that our results are generic and will be applicable to other combinations of septins which have yet to be characterized experimentally (Kinoshita, 2003). More than this, our data rationalize an observation which was previously difficult to explain; namely that of why human septin core complexes apparently left exposed the very stable G interface whilst yeast core complexes do not. We have shown that, in fact, at high salt concentrations, they both leave NC interfaces exposed.

It is interesting to note that septin polymerization from either of the proposed core complexes (2-6-7-7-6-2 or 7-6-2-2-6-7) leads to the same sequence of monomers along the filament. Nevertheless, the way in which filaments assemble physiologically may be critically dependent on the nature of the core complex and some aspects of septin physiology may therefore need to be reconsidered in the light of the discovery reported here.

3 | MATERIAL AND METHODS

3.1 | Plasmid construction

cDNAs encoding full-length human SEPT2 (GenBank NM_004404), SEPT5 (GenBank NM_002688), SEPT6 (GenBank NM_145799), and SEPT7 (GenBank NM_001788), were amplified from a fetal human brain cDNA library (Clontech) by PCR and checked by automated sequencing.
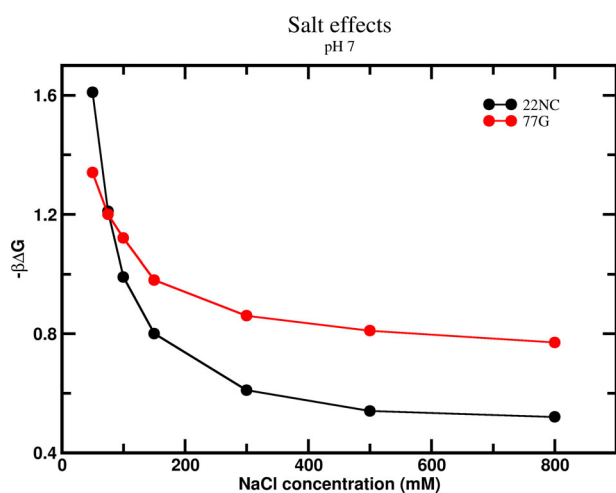

FIGURE 4 Theoretical calculations of the stability of the SEPT2–SEPT2 NC interface (black curve) and the SEPT7–SEPT7 G interface (red) as a function of NaCl concentration [Color figure can be viewed at wileyonlinelibrary.com] [Color figure can be viewed at wileyonlinelibrary.com]
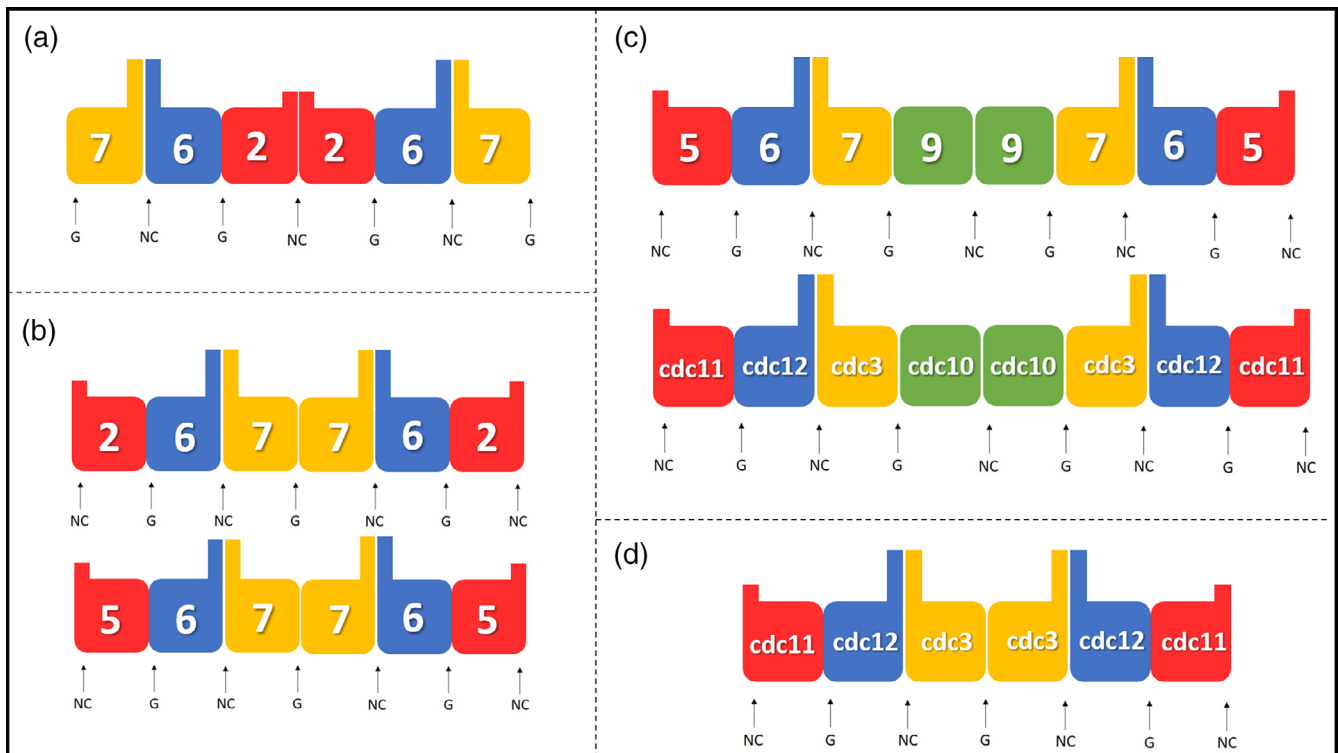
FIGURE 5 Proposition for human septin positions in the heterocomplexes. (a) The original proposed arrangement for the SEPT2–SEPT6–SEPT7 complex as described in the literature; (b) proposed arrangement for the 2-6-7 and 5-6-7 complexes based on the results described here; (c) proposal for the arrangement of the octameric core particle (including the SEPT9 group) and its comparison with the *Saccharomyces cerevisiae* septin complex (Bertin et al., 2008); (d) the hexameric particle from *S. cerevisiae* lacking cdc10 (McMurray et al., 2012). Arrows indicate NC and G interfaces [Color figure can be viewed at wileyonlinelibrary.com] [Color figure can be viewed at wileyonlinelibrary.com]

Complexes (5-6-7 or 2-6-7) were coexpressed using two bicistronic vectors, pETDuet™-1 and pRSFDuet™-1 (NOVAGEN).

For the first expression vector construct, the cDNA encoding SEPT7 (residues 29–437) was subcloned into pETDuet™-1, using *BamH*I and *Pst*I restriction sites. SEPT7 was therefore produced in fusion with an N-terminal 6xHis-tag allowing for its purification by metal affinity chromatography, together with its interaction partners in both complexes (5-6-7 and 2-6-7).

For the second expression vector construct, the coding sequence for SEPT5 (or SEPT2) was inserted into pRSFDuet™-1, using *EcoR*I e *Sal*I restriction sites (in both cases). Subsequently, the CDS for SEPT6 was subcloned (using *EcoR*V and *Xho*I restriction sites) into the same plasmid already containing SEPT5 (or SEPT2). The final constructs permitted the coexpression of SEPT6 together with SEPT5 (or SEPT2).

Additionally, a third set of constructs with the same combination of septins was based on a modified plasmid pRSFDuetTM-1. The modification consisted in exchanging the CDS of the His-tag by that of MBP (Maltose Binding Protein), allowing the expression of the target proteins in N-terminal fusion with MBP.

3.2 | Protein expression and purification

Expression of the protein complexes was performed in *E. coli* Rosetta (DE3) as host cells. Since the protocols developed for the expression and purification of both complexes were distinct in some details, a protocol for the SEPT5–SEPT6–SEPT7 complex will be presented first, followed by the changes made in the case of the SEPT2–SEPT6–SEPT7 complex.

3.2.1 | SEPT5–SEPT6–SEPT7 complex

Fifty milliliter from an overnight culture harboring both expression plasmids (pETDuet_SEPT7 and pRSFDuet_SEPT5-SEPT6) were inoculated into 2 L of Terrific Broth medium, augmented with ampicillin (50 μg/mL), kanamycin (30 μg/mL), and chloramphenicol (34 μg/mL). Cells were grown at 37 °C while shaking at 250 rpm. When the OD_{600nm} reached 1–1.2, the temperature was decreased to 20 °C for 1 hr. Expression was induced with 0.25 mM IPTG (isopropyl-β-D-tiogalactopiranoside) at 20 °C, 200 rpm for 16 hr. Cells were harvested by centrifugation at 6,000*g* for 40 min at 4°C, resuspended in 100 mL buffer A (25 mM Tris–HCl, pH 7.8, containing 500 mM NaCl, 5 mM $MgCl_2$, 5 mM β-mercaptoethanol, 5% [v/v] glycerol), with fresh addition of protease inhibitor cocktail tablets (Roche), in the presence of 0.5 mg/mL lysozyme. The suspension was incubated for 30 min at 4 °C. Cells were disrupted by sonication and centrifuged at 18,000*g* for 30 min at 4 °C. The soluble fraction was loaded onto a column containing 5 mL Ni-NTA superflow resin (Qiagen), pre-equilibrated with buffer A. The column was washed with 7 volumes of buffer A supplemented with 0.1% Triton X-100, followed by

7 volumes of buffer A. The SEPT5–SEPT6–SEPT7 complex was eluted in 50 mL of buffer A containing 400 mM imidazole.

3.2.2 | SEPT2–SEPT6–SEPT7 complex

SEPT2, SEPT6, and SEPT7 were coexpressed simultaneously using similar conditions described above for the SEPT5–SEPT6–SEPT7 complex. Expression was induced with 0.25 mM IPTG (isopropyl-β-D-tiogalactopiranoside) at 18 °C, at 200 rpm, for 16 hr. Cells were harvested by centrifugation at 6,000g for 40 min at 4°C, and resuspended in 60 mL buffer B (25 mM HEPES, pH 7.8, containing 800 mM NaCl, 5 mM MgCl$_2$, 5 mM β-mercaptoethanol, 5% [v/v] glycerol) prior to lysis.

A separate protocol to maximize yields was developed, where SEPT2 and SEPT6 were coexpressed, but SEPT7 was expressed separately, under the same conditions described above. Subsequently, cells from each culture were harvested by centrifugation at 5,000g for 10 min at 4°C, mixed and resuspended in 60 mL buffer B, to allow the complex assembly immediately after the cell lysis.

For both experiments using the 2-6-7 complex, the cells were disrupted by sonication and centrifuged at 10,000g for 60 min at 4 °C. The soluble fraction was loaded onto a HisTrap HP 5 mL column (GE Healthcare), pre-equilibrated with buffer B and then washed with 6 volumes of buffer B supplemented with 30 mM imidazole. The SEPT2–SEPT6–SEPT7 complex was eluted during a linear gradient of 25 mL of buffer B ramping from 30 to 500 mM imidazole.

After the affinity chromatography, the purified complexes were concentrated and loaded onto a Superdex 200 10/300 GL column (GE Healthcare) pre-equilibrated with buffer B. The purity and integrity of all the septin complexes were analyzed on 12% SDS-PAGE. Fractions containing the complex were concentrated to 1 mg/mL and aliquots of 20 μL were frozen in liquid N$_2$ and stored at −80 °C.

The complexes containing MBP followed similar protocols, except for the addition of a chromatography step (amylose affinity column, New England Biolabs) according to the manufacturer's instructions prior to the size exclusion chromatography.

3.3 | Mass spectrometry

The individual components of the complex were identified by LC–MS/MS analysis on an ESI-micrOTOF-Q II 10234 mass spectrometer (Bruker Daltonics) and the data analyzed with MASCOT, available from http://www.matrix science.com/search_form_select.html.

3.4 | Analysis of nucleotide content

Nucleotides were extracted from the purified protein complex samples according to the method described by Seckler et al., with some modifications (SECKLER, WU, & TIMASHEFF, 1990). Ice-cold HClO$_4$ (final concentration 0.5 M) was added to the purified SEPT5–SEPT6–SEPT7 complex in buffer containing 300 mM NaCl, followed by incubation on ice for 10 min. After centrifugation at 16,000g at 4 °C for 10 min, the supernatant was buffered and neutralized with 100 μL of

KOH 3 M, 100 μL K$_2$HPO$_4$ 1 M, and 20 μL acetic acid to a final concentration of 0.5 M. After a centrifugation step at 16,000g at 4 °C for 10 min, the nucleotides were analyzed using anion exchange chromatography on a Protein Pack DEAE 5 PW 7.5 mm × 7.5 cm column (Waters) driven by a Waters 2695 chromatography system. The column was equilibrated in 50 mM Tris at pH 8.0 and 150 μL of each sample were loaded into the system. Elution was performed using a linear NaCl gradient (0.1–0.45 M in 10 min) at a flow rate of 1 mL/min at room temperature. The absorbance was monitored at 253 nm. As a reference, a mixture of 5 μM GDP and 5 μM GTP was used in the same buffer.

3.5 | EM and image processing

Purified septin complexes were diluted to 0.02 mg/mL using the final purification buffer so as to maintain the NaCl concentration between 500 and 800 mM, adsorbed for 1 min onto glow-discharged, ultrathin carbon film supported by lacey carbon on a copper grid (Ted Pella). The samples were washed in a drop of deionized water and stained in two drops of 2% uranyl acetate, without addition of a fixative. Micrographs of SEPT5–SEPT6–SEPT7 complexes (with or without MBP) were recorded using an F416 camera (TVIPS, Germany) with a JEM-2100 (JEOL, Japan) microscope operated at 200 kV with a pixel size of 1.78 Å. Micrographs of MBP-SEPT2–SEPT6–SEPT7 were taken on a Talos Arctica (Thermo Fisher Scientific, USA) and were recorded using a Ceta camera with a pixel size of 2.51 Å at a defocus range of 1–3 mm underfocus. Images of high-salt (500 mM) samples incubated with mouse monoclonal anti-SEPT5 were taken on a Talos F200C (Thermo Fisher Scientific) microscope at 200 kV and were also recorded using a Ceta camera with a pixel size of 2.6 Å. Imagic4D software (Image Science, Germany) was used for image processing (van Heel et al., 2012). Class averages of selected particles were computed after alignment by classification and subsequent rounds of multivariate statistical analysis (MSA) using selected masks (Afanasyev et al., 2017; van Heel, Portugal, & Schatz, 2016). For better visualization of the MBP location, due to the flexible linker, one of the masks used was constructed as a rectangle on the hexameric complex, so that only information from the MBP was used for classification. For simplicity, during data processing a mask was also employed to guarantee that the MBP always appeared in the upper portion of the image. The average number of members per class was 30 particles.

3.6 | Structural analysis

The structural characteristics of the G and NC interfaces were analyzed with the PISA server allied to visual inspection (Krissinel & Henrick, 2007). In the case of the G interface, which resides between two copies of SEPT7 within a mature filament, the recently determined crystal structure of human SEPT7 at 1.73 Å resolution (PDB ID 6N0B) was used. For the NC interface a chimeric model was built from two previously reported crystal structures for SEPT2 (PDB IDs 2QNR and 2QA5). The higher resolution structure (PDB ID 2QNR) was used as a main model with the incorporation of the α$_0$ helix

(polybasic region) from PDB ID 2QA5 included after structural super-position followed by structure completion and regularization with MODELLER 9.0.

Using a constant-pH Coarse Grain scheme previously devised to study protein–protein interactions, (Barroso Da Silva, Pasquali, Derreumaux, & Dias, 2016; Delboni & Barroso da Silva, 2016; Forsman, Chatterton, Åkesson, Persson, & Lund, 2010) the two interfaces were also submitted to a complexation study at pH 7 under several different salt concentrations (50, 75, 100, 150, 300, 500, and 800 mM) at 298 K. Titratable groups were allowed to change their protonation states according to a fast proton titration scheme shown to be accurate in reproducing experimental pKa shifts (Barroso da Silva & Mackernan, 2017). Guanosine phosphate molecules were modeled based on the guanine nucleobase titration model (Barroso da Silva, Derreumaux, & Pasquali, 2018) with the inclusion of phosphates. The number of MC steps for production was at least 10^7 after equilibration. The protein–protein radial distribution function [$g(r)$] was sampled with a bin size of 1 Å. From this function, the angularly averaged potential of mean force ($\beta w(r) = -\ln [g(r)]$, where $\beta = 1/k_BT$ and k_B and is the Boltzmann constant) between the centers of mass of the two chains was obtained with low noise, and used to estimate the free energy of complexation (ΔG) under each physicochemical condition. Three independent runs were performed to assure sampling convergence.

CONFLICT OF INTEREST

The authors declare that they have no conflicts of interest.

DATA AVAILABILITY

Original data are available from the authors on reasonable request.

ORCID

Richard C. Garratt https://orcid.org/0000-0002-2016-3179
Ana P. U. Araujo https://orcid.org/0000-0001-5455-084X

REFERENCES

Afanasyev, P., Seer-Linnemayr, C., Ravelli, R. B. G., Matadeen, R., De Carlo, S., Alewijnse, B., ... van Heel, M. (2017). Single-particle cryo-EM using alignment by classification (ABC): The structure of *Lumbricus terrestris* haemoglobin. *IUCrJ*, *4*(5), 678–694. https://doi.org/10.1107/S2052252517010922

Barroso da Silva, F. L., Derreumaux, P., & Pasquali, S. (2018). Protein-RNA complexation driven by the charge regulation mechanism. *Biochemical and Biophysical Research Communications*, *498*(2), 264–273. https://doi.org/10.1016/j.bbrc.2017.07.027

Barroso da Silva, F. L., & Mackernan, D. (2017). Benchmarking a fast proton titration scheme in implicit solvent for biomolecular simulations. *Journal of Chemical Theory and Computation*, *13*(6), 2915–2929. https://doi.org/10.1021/acs.jctc.6b01114

Barroso Da Silva, F. L., Pasquali, S., Derreumaux, P., & Dias, L. G. (2016). Electrostatics analysis of the mutational and pH effects of the N-terminal domain self-association of the major ampullate spidroin. *Soft Matter*, *12*(25), 5600–5612. https://doi.org/10.1039/c6sm00860g

Barth, P., Schoeffler, A., & Alber, T. (2008). Targeting metastable coiled-coil domains by computational design. *Journal of the American Chemical Society*, *130*(36), 12038–12044. https://doi.org/10.1021/ja802447e

Beise, N., & Trimble, W. (2011). Septins at a glance. *Journal of Cell Science*, *124*(24), 4141–4146. https://doi.org/10.1242/jcs.087007

Bertin, A., McMurray, M. A., Grob, P., Park, S., Iii, G. G., Patanwala, I., ... Nogales, E. (2008). *Saccharomyces cerevisiae* septins: Supramolecular organization of heterooligomers and the mechanism of filament assembly. *Proceedings of the National Academy of Sciences*, *105*(24), 8274–8279. https://doi.org/10.1073/pnas.0803330105

Bridges, A. A., Zhang, H., Mehta, S. B., Occhipinti, P., & Tani, T. (2014). Septin assemblies form by diffusion-driven annealing on membranes. *Proceedings of the National Academy of Sciences*, *111*(6), 2146–2151. https://doi.org/10.1073/pnas.1314138111

Caudron, F., & Barral, Y. (2009). Septins and the lateral compartmentalization of eukaryotic membranes. *Developmental Cell*, *16*(4), 493–506. https://doi.org/10.1016/j.devcel.2009.04.003

de Marques, I. A., Valadares, N. F., Garcia, W., Damalio, J. C. P., Macedo, J. N. A., de Araújo, A. P. U., ... Garratt, R. C. (2012). Septin C-terminal domain interactions: Implications for filament stability and assembly. *Cell Biochemistry and Biophysics*, *62*(2), 317–328. https://doi.org/10.1007/s12013-011-9307-0

Delboni, L. A., & Barroso da Silva, F. L. (2016). On the complexation of whey proteins. *Food Hydrocolloids*, *55*, 89–99. https://doi.org/10.1016/j.foodhyd.2015.11.010

Field, C. M., Al-Awar, O., Rosenblatt, J., Wong, M. L., Alberts, B., & Mitchison, T. J. (1996). A purified drosophila septin complex forms filaments and exhibits GTPase activity. *The Journal of Cell Biology*, *133*(3), 605–616. https://doi.org/10.1083/jcb.133.3.605

Forsman, J., Chatterton, D. E. W., Åkesson, T., Persson, B. A., & Lund, M. (2010). Molecular evidence of stereo-specific lactoferrin dimers in solution. *Biophysical Chemistry*, *151*(3), 187–189. https://doi.org/10.1016/j.bpc.2010.06.005

Frazier, J. A., Wong, M. L., Longtine, M. S., Pringle, J. R., Mann, M., Mitchison, T. J., & Field, C. (1998). Polymerization of purified yeast septins: Evidence that organized filament arrays may not be required for septin function. *The Journal of Cell Biology*, *143*(3), 737–749. https://doi.org/10.1083/jcb.143.3.737

Gladfelter, A. S., Pringle, J. R., & Lew, D. J. (2001). The septin cortex at the yeast mother—Bud neck. *Current Opinion in Microbiology*, *4*, 681–689. https://doi.org/10.1016/S1369-5274(01)00269-7

John, C. M., Hite, R. K., Weirich, C. S., Daniel, J., Faty, M., Schlapfer, D., ... Steinmetz, M. O. (2007). The *Caenorhabditis elegans* septin complex is nonpolar. *The EMBO Journal*, *26*(14), 3296–3307. https://doi.org/10.1038/sj.emboj.7601775

Kim, M. S., Froese, C. D., Estey, M. P., & Trimble, W. S. (2011). SEPT9 occupies the terminal positions in septin octamers and mediates polymerization-dependent functions in abscission. *Journal of Cell Biology*, *195*(5), 815–826. https://doi.org/10.1083/jcb.201106131

Kinoshita, M. (2003). Assembly of mammalian septins. *Journal of Biochemistry*, *134*(4), 491–496. https://doi.org/10.1093/jb/mvg182

Krissinel, E., & Henrick, K. (2007). Inference of macromolecular assemblies from crystalline state. *Journal of Molecular Biology*, *372*, 774–797. https://doi.org/10.1016/j.jmb.2007.05.022

Lam, M., & Calvo, F. (2018). Regulation of mechanotransduction: Emerging roles for septins. *Cytoskeleton*, *76*(1), 115–122. https://doi.org/10.1002/cm.21485

Lukoyanova, N., Baldwin, S. A., & Trinick, J. (2008). 3D reconstruction of mammalian septin filaments. *Journal of Molecular Biology*, *376*, 1–7. https://doi.org/10.1016/j.jmb.2007.11.029

Martínez, C., Corral, J., Dent, J. A., Sesma, L., Vicente, V., & Ware, J. (2006). Platelet septin complexes form rings and associate with the microtubular network. *Journal of Thrombosis and Haemostasis*, *4*(6), 1388–1395. https://doi.org/10.1111/j.1538-7836.2006.01952.x

McMurray, M. A., Bertin, A., Iii, G. G., Lam, L., Nogales, E., & Thorner, J. (2012). Septin filament formation is essential in budding yeast. *Developmental Cell*, *20*(4), 540–549. https://doi.org/10.1016/j.devcel.2011.02.004.Septin

Mostowy, S., & Cossart, P. (2012). Septins: The fourth component of the cytoskeleton. *Nature Reviews. Molecular Cell Biology*, *13*(3), 183–194. https://doi.org/10.1038/nrm3284

Nagata, K., Asano, T., Nozawa, Y., & Inagaki, M. (2004). Biochemical and cell biological analyses of a mammalian septin complex, Sept7/9b/11. *Journal of Biological Chemistry*, *279*(53), 55895–55904. https://doi.org/10.1074/jbc.M406153200

Nakahira, M., Macedo, J. N. A., Seraphim, T. V., Cavalcante, N., Souza, T. A. C. B., Damalio, J. C. P., ... Kobarg, J. (2010). A draft of the human septin interactome. *PLoS One*, *5*(11), e13799. https://doi.org/10.1371/journal.pone.0013799

Neubauer, K., & Zieger, B. (2017). The mammalian septin interactome. *Frontiers in Cell and Developmental Biology*, *5*, 1–9. https://doi.org/10.3389/fcell.2017.00003

Nishihama, R., Onishi, M., & Pringle, J. R. (2011). New insights into the phylogenetic distribution and evolutionary origins of the septins Ryuichi. *Biological Chemistry*, *392*, 681–687. https://doi.org/10.1038/jid.2014.371

Pan, F., Malmberg, R. L., & Momany, M. (2007). Analysis of septins across kingdoms reveals orthology and new motifs. *BMC Evolutionary Biology*, *7*(103), 1–17. https://doi.org/10.1186/1471-2148-7-103

Sala, F. A., Valadares, N. F., Macedo, J. N. A., Borges, J. C., & Garratt, R. C. (2016). Heterotypic coiled-coil formation is essential for the correct assembly of the Septin Heterofilament. *Biophysical Journal*, *111*(12), 2608–2619. https://doi.org/10.1016/j.bpj.2016.10.032

Sandrock, K., Bartsch, I., Bläser, S., Busse, A., Busse, E., & Zieger, B. (2011). Characterization of human septin interactions. *Biological Chemistry*, *392*(8–9), 751–761. https://doi.org/10.1515/BC.2011.081

Seckler, R., Wu, G. M., & Timasheff, S. N. (1990). Interactions of tubulin with guanylyl-(beta-gamma-methylene)diphosphonate. Formation and assembly of a stoichiometric complex. *Journal of Biological Chemistry*, *265*(13), 7655–7661.

Sellin, M. E., Sandblad, L., Stenmark, S., Gullberg, M., & Kellogg, D. R. (2011). Deciphering the rules governing assembly order of mammalian septin complexes. *Molecular Biology of the Cell*, *22*(17), 3152–3164. https://doi.org/10.1091/mbc.E11-03-0253

Sirajuddin, M. (2007). *Structural studies on mammalian septins—New insights into filament formation*. Germany: Universität Dortmund.

Sirajuddin, M., Farkasovsky, M., Hauer, F., Kuhlmann, D., Macara, I. G., Weyand, M., ... Wittinghofer, A. (2007). Structural insight into filament formation by mammalian septins. *Nature*, *449*, 311–117. https://doi.org/10.1038/nature06052

Valadares, N. F., Pereira, H. d.' M., Araujo, A. P. U., & Garratt, R. C. (2017). Septin structure and filament assembly. *Biophysical Reviews*, *9*, 481–500. https://doi.org/10.1007/s12551-017-0320-4

van Heel, M., Portugal, R. V., Rohou, A., Linnemayr, C., Bebeacua, C., Schmidt, R., ... Schatz, M. (2012). Four-dimensional cryo-electron microscopy at quasi-atomic resolution: IMAGIC 4D. In M. G. R. E. Arnold & D. M. Himmel (Eds.), *International tables for crystallography* (2nd ed., pp. 624–628), Chester, England: IUCr/Wiley. https://doi.org/10.1107/97809553602060000111

van Heel, M., Portugal, R. V., & Schatz, M. (2016). Multivariate statistical analysis of large datasets: Single particle electron. *Open Journal of Statistics*, *6*, 701–739. https://doi.org/10.4236/ojs.2016.64059

Versele, M., Shulewitz, M. J., Cid, V. J., Bahmanyar, S., Chen, R. E., Barth, P., ... Thorner, J. (2004). Protein–protein interactions governing septin heteropentamer assembly and septin filament organization in *Saccharomyces cerevisiae*. *Molecular Biology of the Cell*, *15*, 4568–4583. https://doi.org/10.1091/mbc.E04

Weirich, C. S., Erzberger, J. P., & Barral, Y. (2008). The septin family of GTPases: Architecture and dynamics. *Nature Reviews. Molecular Cell Biology*, *9*(6), 478–489. https://doi.org/10.1038/nrm2407

Zent, E., & Wittinghofer, A. (2014). Human septin isoforms and the GDP-GTP cycle. *Biological Chemistry*, *395*(2), 169–180. https://doi.org/10.1515/hsz-2013-0268

Zeraik, A. E., Pereira, H. M., Santos, Y. V., Brandão-neto, J., Spoerner, M., Santos, M. S., ... Demarco, R. (2014). Crystal structure of a *Schistosoma mansoni* septin reveals the phenomenon of strand slippage in septins dependent on the nature of the bound nucleotide. *The Journal of Biological Chemistry*, *289*(11), 7799–7811. https://doi.org/10.1074/jbc.M113.525352